Article

Special Characteristics and Stability Analysis of Bank Slope Deposits with Special Geotechnical Structures in High and Cold Valleys

Shuyu Wu [1,2], Daru Hu [1,2] and Tao Wen [3,*]

1   Power China Guiyang Engineering Corporation, Ltd., Guiyang 550081, China
2   China Guiyang Engineering Corporation Geotechnical Engineering Co., Ltd., Guiyang 550081, China
3   School of Geosciences, Yangtze University, Wuhan 430100, China
*   Correspondence: wentao200840@yangtzeu.edu.cn

Abstract: Due to the special internal and external dynamic action of the Qinghai-Tibet Plateau, the high and cold valleys are typically characterized by high-steep terrain, dry and cold climate, lithologic diversity, complex geological structure, and frequent occurrence of earthquakes. In this study, the types of special geotechnical structures of bank slope deposits in high and cold valleys are summarized based on field investigation, field and laboratory tests, and numerical simulation. These special deposits include colluvial-deluvial deposits, terrace deposits, early debris flow deposits, and landslide deposits. The formation mechanism, physical and mechanical properties, and stability analysis of these deposits were studied. The results show that the formation mechanism of various deposits is different, which is closely related to the intense geological tectonic action, the weathering and unloading action intensified by freezing and thawing cycles, and the special rock and soil structure in the high and cold valleys. Different material compositions have obvious effects on the physical and mechanical properties of the deposits, thus affecting the stability and deformation characteristics of the deposits. Under natural and saturated conditions, the stability of different types of the deposits is different, which is mainly related to the special geotechnical structure of various deposits. Compared with that before the reservoir impoundment, the stability factor of various deposits after the reservoir impoundment is significantly reduced. The performances can be provided as a reference for evaluating the stability of bank slope deposits in high and cold valleys.

Keywords: high and cold valley; special geotechnical structure; deposits; stability analysis; reservoir impoundment

1. Introduction

The Qinghai-Tibet Plateau is regarded as the Earth's third pole characterized by intense tectonic activities, a dry and cold climate, deeply incised valleys, and frequent occurrence of earthquakes [1,2]. Various deposits in high and cold valleys are widely distributed on both banks of the river due to complex and adverse geological environments, which have large burial depths and large volumes [3,4]. In particular, since the construction of the hydropower project in the southeast of the Qinghai-Tibet Plateau, the change of the physical and mechanical parameters and stability of the bank slope deposit after impoundment is the biggest change in the geological environment of the hydropower station area [5,6]. In the complex topographic and geological background of the high and cold valleys, the change of the geological environment has more particularity, which is very likely to lead to the revival, deformation and destruction of the special deposits, bringing new challenges to the project construction [7,8].

Colluvial-deluvial deposits have numerous gravel, sand, and loose materials, characterized by a weak structure, high erodibility, low cohesion, and poor stability [9–13]. The deposits disintegrate rapidly when they are immersed, then abundant sediments are

generated and flow out of the gully through scour channels [14–17]. Therefore, numerous sediments released from the colluvial-deluvial deposits can destroy the area downhill of a collapsing gully [18,19]. The erosion of the colluvial-deluvial deposits should be taken into consideration. However, the special characteristics and formation mechanism by which the deposits are eroded have not been thoroughly investigated and still need in-depth study on the high and cold valleys. In the high and cold valleys, fluvial terraces that can supply information about the response of a river system to tectonic and climate changes are important landforms [20,21]. However, the influences of the tectonic and climate changes on the spatial distribution of the terrace deposits remain unclear [22]. The greatest challenge is to interpret terrace records from regions where climate changes are overlaid on spatial and temporal variations in tectonically driven rock uplift [23]. Furthermore, the investigation on the thickness of the terrace deposits is not detailed in high and cold valleys. In the Qinghai-Tibet Plateau, numerous debris flow deposits are developing from the erosion of the colluvial-deluvial deposits and landslide deposits [24–26]. These deposit materials are in an understable state in the dry season while they can offer source materials for debris flow deposits in the wet season [27]. Due to high-steep terrain in the valleys, a large landslide movement with high velocity can easily transform into high-speed and long-distance debris flow [28]. Complex geological environments cause large landslides in the Three Parallel Rivers (including Jinsha River, Lancang River, and Nujiang River) area at the junction of Tibet and Sichuan in the Qinghai-Tibet Plateau, and complex formation mechanism of landslide deposits in different regions [1,2]. These landslide deposits are mainly distributed along major rivers due to the existence of steep deeply incised valleys [1]. The instability of these landslides will destroy everything that they encounter, and results in catastrophic consequences [2]. However, few studies are paying attention to the distribution of the landslide deposits in the high and cold valleys and their formation mechanism.

In China, more and more hydropower stations are being built in the high and cold valleys of the Qinghai-Tibet Plateau. Numerous deposits and unstable slopes exist in the construction process of the hydropower stations and during the reservoir impoundment. A good understanding of the unstable deposit distribution and corresponding deformation and failure characteristics is helpful for the prevention and reduction of the unstable deposits. In this study, the formation mechanism, physical and mechanical properties, and stability analysis of the bank slope deposits with the special geotechnical structure in the high and cold valleys on the Qinghai-Tibet Plateau are presented based on the field investigations of several hydropower stations, field and laboratory tests of soil mass, and numerical simulations of the deposits. Furthermore, the influences of the reservoir impoundment on the stability of bank slope deposits in the high and cold valleys are also revealed.

2. Study Area

2.1. Location of the High and Cold Valleys

The research objects in this study are the special geotechnical structures in high and cold valleys in the Qinghai-Tibet Plateau. These special structures including colluvial-deluvial deposits, terrace deposits, debris flow deposits, and landslide deposits are located in the Three Parallel Rivers area at the junction of Tibet and Sichuan in the Qinghai-Tibet Plateau, as shown in Figure 1. These deposits are mainly in the reservoir area of the RM, GD, and CB hydropower stations. The Qinghai-Tibet Plateau is located in the western part of China. Being squeezed by the Indian plate to the north-northeast (NNE) and constrained by the eastern and north-eastern boundaries, the Tibetan Plateau is rising continuously. The valleys in this region have some unique characteristics, such as high-steep terrain, dry and cold climate, lithologic diversity, complex geological structure, and frequent occurrences of earthquakes.
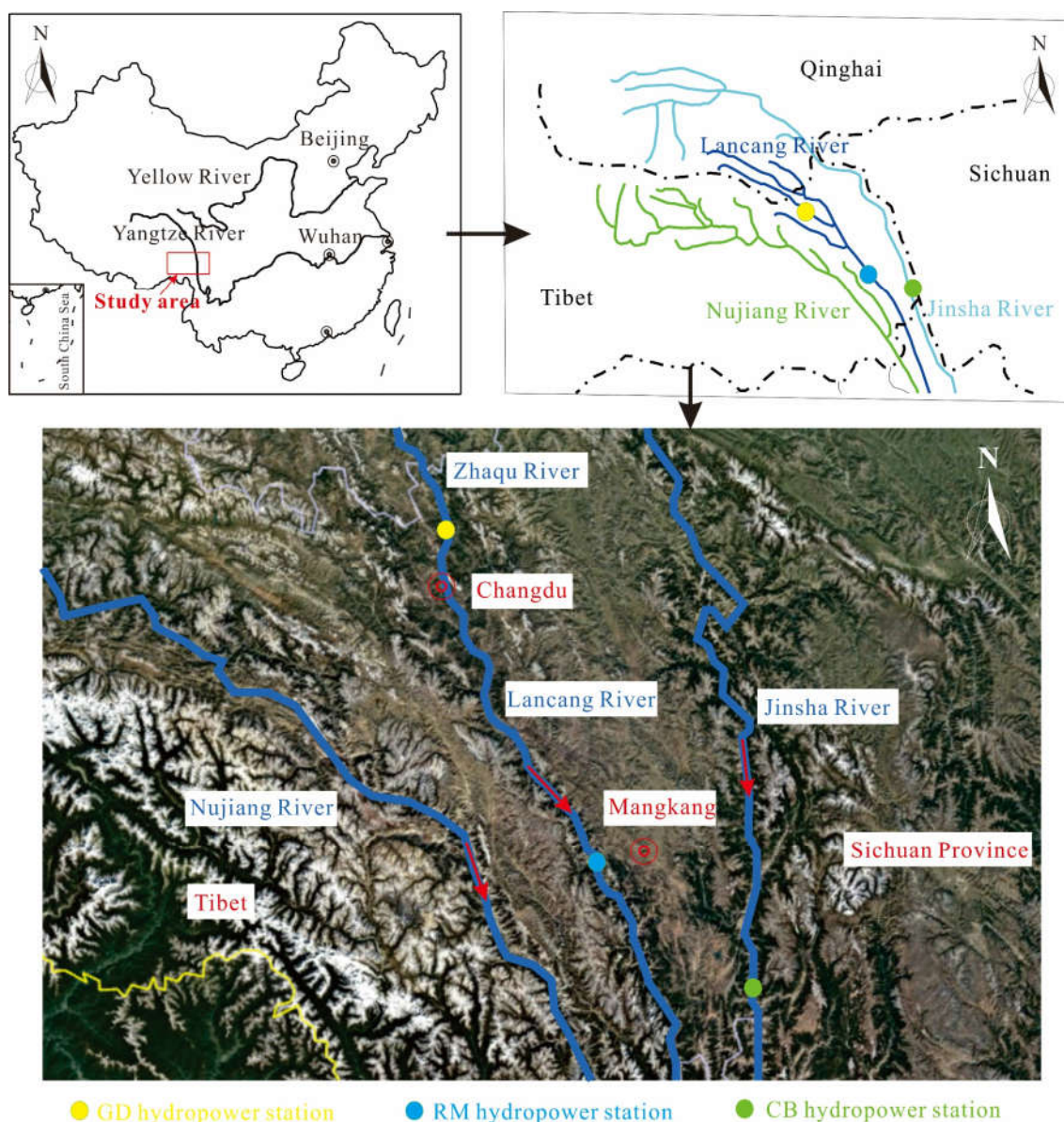
Figure 1. Location of the high and cold valleys.

In the Three Parallel Rivers and Mangkang region on the south-eastern margin of the Qinghai-Tibet Plateau, the average elevation is about 4500 m, and most summits are higher than 5000 m. The elevations of valley bottoms are within the range of 2300–2600 m, and the depths of valleys are generally greater than 2000 m. The slopes of valley sides are within the range of 40–70°, and the annual mean temperature is 5–10°. The highest temperature is 25°, and the lowest temperature is −23°. The annual precipitation is 575 mm, and the maximum daily rainfall is 55 mm.

2.2. Materials Composition

The strata in this region are subdivided into three strata. The western part is the Basu-Zhayu strata, which is dominated by the clastic sedimentary rocks and volcanic rocks deposited in the late Palaeozoic and the late Triassic. The middle part is the Wuqi-Zuogong strata, which is dominated by volcanic rocks deposited from the late Palaeozoic to the Mesozoic. The eastern part is the Changdu-Mangkang strata, which is dominated by the continental red beds formed during the Jurassic and Cretaceous periods of the Mesozoic Era.

2.3. Structural Geological Characteristics

The tectonics in the study area are very complex, with strong structural deformation and developed fault structures. The distribution of major faults in the region is shown in Figure 2, mainly in the NNW-NS direction and the NW-NWW direction, followed by the NE-NNE direction. There are obvious differences in the regional structural attributes, scale, activity age, activity intensity, etc. The NNW-NS direction fault is the main fault in the area, which is large in scale, mainly including the Nujiang fault zone, the Lancang River fault zone, and the Jinshajiang fault zone. The activity of the fault is characterized by segmentation, which can be divided into south and north segments. The latest activity age of the north segment of the fault is mainly the late Pleistocene, and the latest activity age of the south segment of the fault is mainly the middle Pleistocene. The NW-NWW direction faults are large in scale, some of them are deep and large faults, and thrust and thrust strike-slip faults. The latest active ages of these faults are different periods of the Quaternary period, especially in the late period, and large earthquakes with a magnitude above 7 have occurred many times. The Jiali fault, Bianba-Luolong fault, Xieba fault, Semuxiong fault, Deqin-Zhongdian fault, and Litang fault are all Holocene active faults. The NE-NNE direction fault is mainly distributed in the northeast of the region and belongs to the Holocene active fault. The fault zone has experienced an earthquake of magnitude 7 or above. The typical representative of the fault zone is the Batang fault.
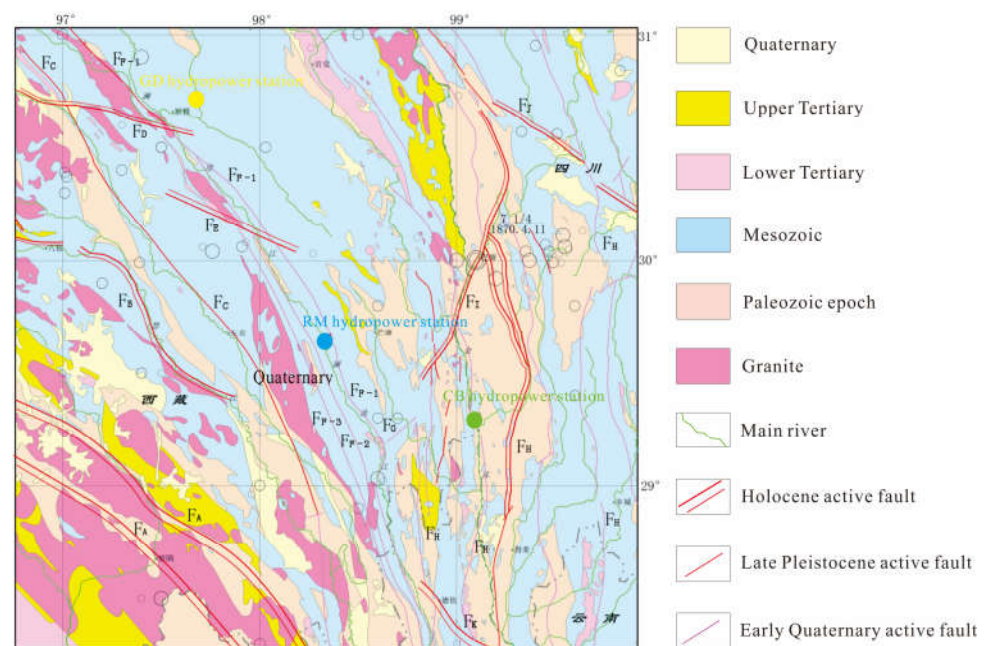

Figure 2. Distribution of main structures in the study area.

3. Case Studies

According to the results of field engineering investigations performed in many hydropower station areas, most of the typical slope deposits in the high and cold valley region are not composed of materials from a single origin but have been formed by the accretion of mixed materials from multiple origins. These typical deposits have certain special geotechnical structures and formation mechanisms. Herein, there are mainly four types of bank slope deposits with special geotechnical structures that are most closely related to reservoir water storage. These four deposits include colluvial-deluvial deposits, terrace deposits, early debris flow deposits, and landslide deposits, which are described and discussed in this study separately.

3.1. Colluvial-Deluvial Deposits

3.1.1. Characteristics of Deposits

Figure 3 presents a typical remote sensing image of colluvial-deluvial deposits in high and cold valleys. According to geological investigations, Rongsong (RS) deposit is distributed along the Lancang river over a distance of about 1.4 km, with a width of 700 m perpendicular to the river direction, and a top-bottom elevation difference of 500–600 m. The maximum depth of the deposit is about 100 m, and the volume is about 4700×10^4 m^3. The formation mechanism is summarized as follows, as shown in Figure 3b:
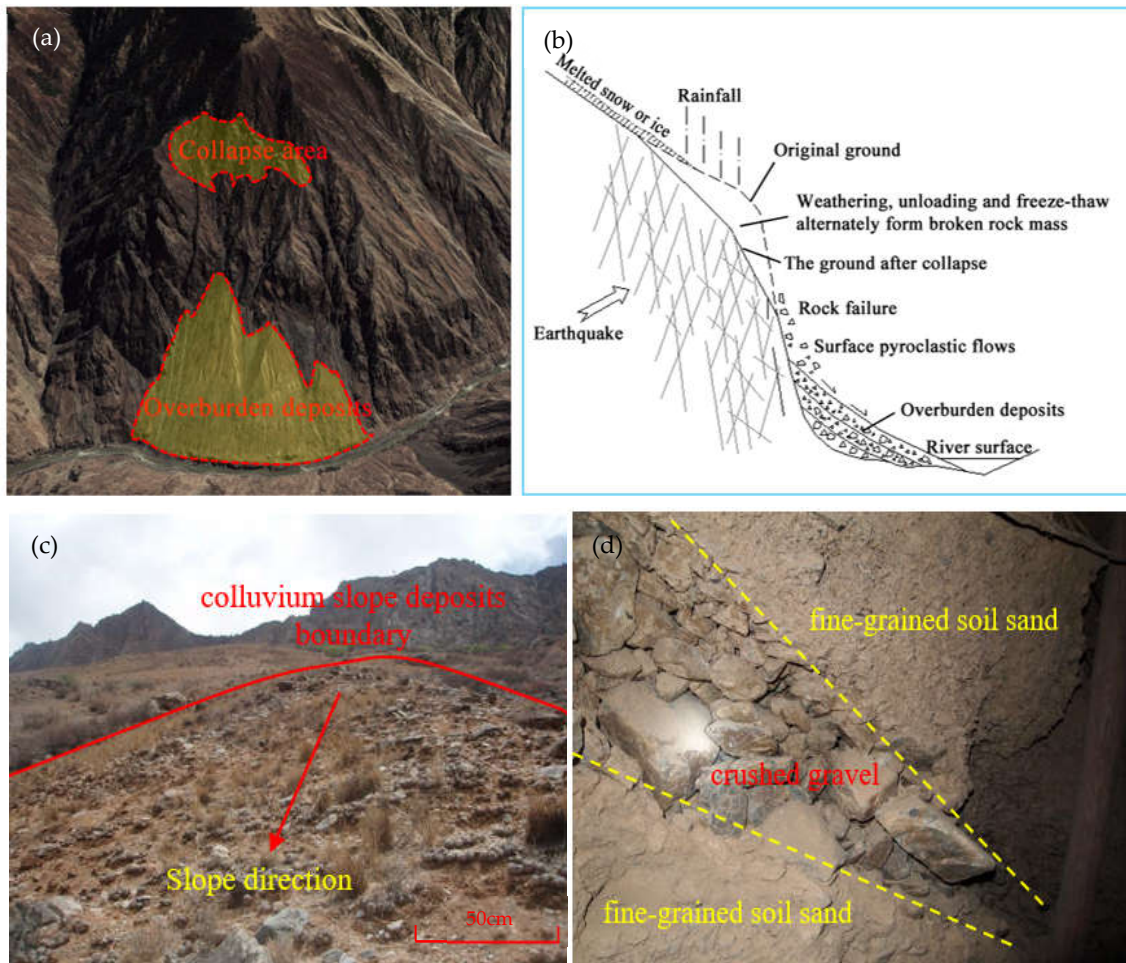

Figure 3. Colluvial-deluvial deposits in high and cold valleys: (**a**) Remote sensing image; (**b**) Engineering geological profile; (**c**) Surface deposits; (**d**) Deep deposits.

The rock mass of the bank slope is affected by its structure to form fissured rock mass. The valley is cut down to form a high and steep free face. At the same time, the stress is released, causing the rock mass to be unloaded and pulled apart. The alternating action of weathering, rainfall, and freezing–thawing aggravates the loosening and deformation of the rock mass. Under the action of a rainstorm, ice and snow melting, and earthquake triggering, the rock mass produces a large deformation. This causes the rock mass to collapse and roll down, and it accumulates at the foot of the slope, forming colluvial deposits mainly composed of rubble. The surface flow is formed by surface rainfall and melting of snow and ice on the slope surface, and the upper rock blocks are transported downward to form slope deposits dominated by gravelly soil. The colluvial-deluvial deposits alternately and intermingled accumulate to a certain thickness to form accumulations.

The colluvial-deluvial deposits contain rubbles of varying sizes and with apparent edges and corners. Compared with the colluvial-deluvial deposits in warm and humid

regions at low altitudes, those in the high and cold valley regions have more special characteristics in terms of rock-soil structure as described below.

(a) The high and cold valley region is characterized by high regional in-situ stress, strong unloading, freezing–thawing, and weathering effects. Broken rock mass has great depth and wide range. The collapse point at the top of the slope has a wide range and high elevation. The collapse volume of colluvial-deluvial deposits is large.

(b) Under tectonic and seismic actions, the rock masses are fractured noticeably and have many small and hidden joints. For this reason, the rock masses tend to be broken and decomposed in the slumping process, which greatly reduces the sizes of deposited rubbles. As shown in Figure 3c, the grain sizes of most rubbles in this deposit are smaller than 50 cm, and the grain sizes of most broken stones in the deposit are within the range of 6 mm–2 cm.

(c) Due to the scouring and leaching effects of streams formed by seasonal rainfall and melting ice and snow at the slope surface, the fine grain content and the degree of cementation in the upper and middle layers of the slope are different. The layer in the RS deposit can be divided into two main types. The first type is a well cemented, fine-grained muddy gravel layer with high silt and clay content. The second type is a poorly cemented broken gravel layer with low silt and clay content. Due to the existence of these two types of layers, multistage colluvial-deluvial deposits contain inclined, rhythmically deposited layers, as shown in Figure 3d. According to the drift exploration statistics, there are 14 inclined, rhythmically deposited layers in the upper section of this deposit.

3.1.2. Physical and Mechanical Properties

To accurately evaluate the stability of various special deposits under natural conditions and water storage conditions, field and laboratory tests were conducted to obtain the physical and mechanical parameters of the rock and soil mass. The samples of colluvial-deluvial deposits were from the RS deposit, No.7 deposit in the RM Hydropower Station area. In general, these deposits are composed mainly of soil mixtures with giant grains and coarse-grained soil based on grain size and field density tests.

Field shear tests were performed on various deposits from different origins and compositions under natural (2–5% of water content) and saturated (lasts for 24 h) conditions. The tests were conducted through drifts or vertical shafts drilled from the surface. The shortest bottom edge of the samples is no less than 50 cm in length, and the ratio of height to the length of the bottom edge is about 1/2. The deposits performed in the field shear tests include broken gravels in early colluvial-deluvial deposits, fine-grained muddy gravels in early colluvial-deluvial deposits, and sandy gravels in recent colluvial-deluvial deposits. Each deposit has been tested under natural and saturated conditions. For broken gravels in early colluvial-deluvial deposits. The test under the natural condition was conducted at 48–58 m of No.3 drift in the RS deposit, while the test under the saturated condition was conducted in the weakly cemented middle and lower sections of the No.7 deposit. Figure 4a,b present the σ-τ scatter diagrams for field tests in broken gravels in the early colluvial-deluvial deposits. For fine-grained muddy gravels in early colluvial-deluvial deposits, the test under the natural condition was conducted at 25–35 m of No.3 drift in the RS deposit, while the test under the saturated condition was conducted in certain cemented middle and lower sections of the No.7 deposit. Figure 4c,d present the σ-τ scatter diagrams for field tests in fine-grained muddy gravels in the early colluvial-deluvial deposits. For sandy gravels in recent gravels in early colluvial-deluvial deposits, the test under the natural condition was conducted in the upper section of the No.4 deposit. The test under the saturated condition was conducted in the relatively loose surface layer of the No.6 deposit. Figure 4e,f present the σ-τ scatter diagrams for field tests in sandy gravels in recent colluvial-deluvial deposits.
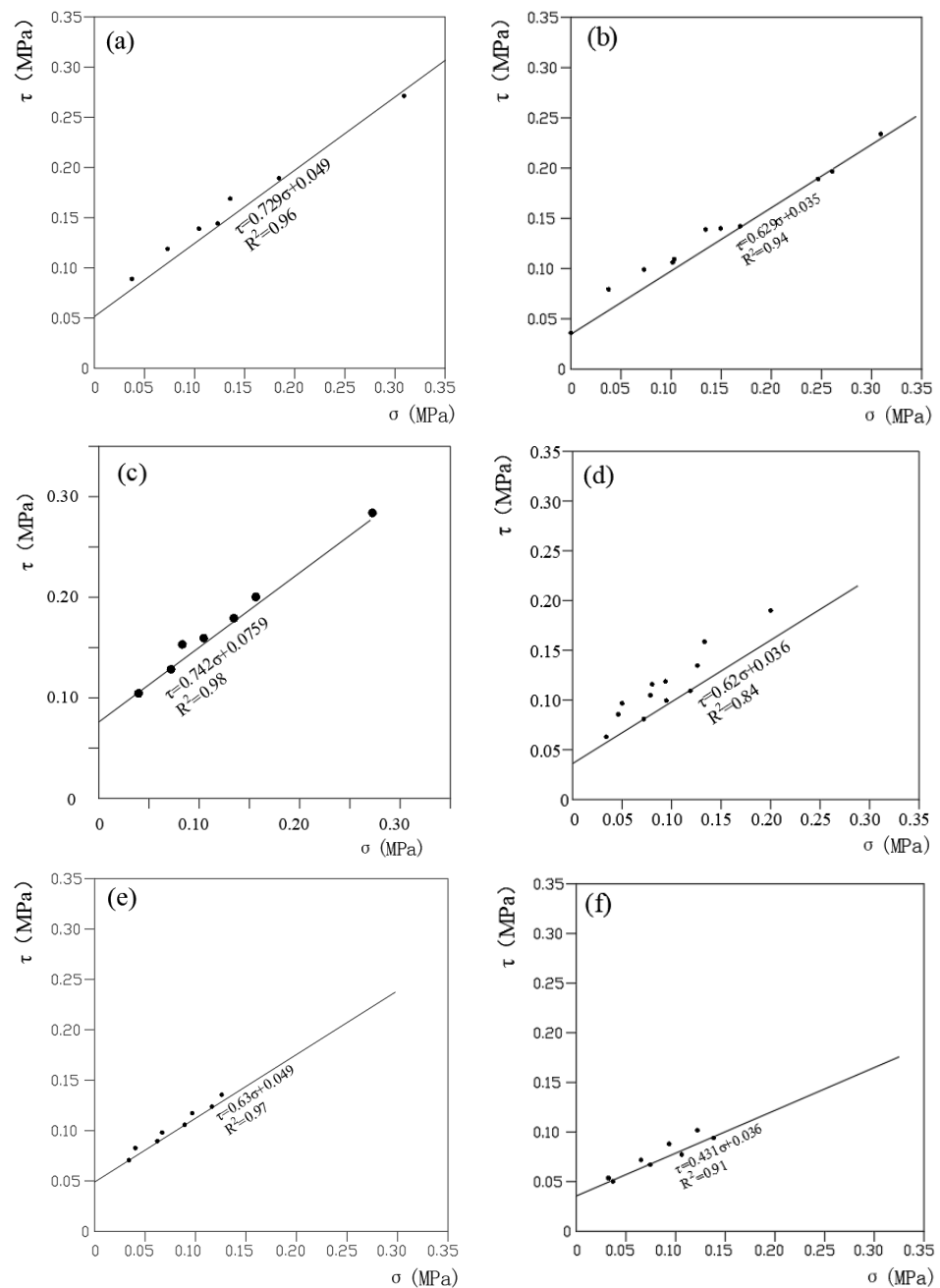
Figure 4. σ-τ scatter diagrams for field tests in colluvial-deluvial deposits: (**a**) Natural conditions on broken gravels; (**b**) Saturation conditions on broken gravels; (**c**) Natural conditions on fine-grained muddy gravels; (**d**) Saturation conditions on fine-grained muddy gravels; (**e**) Natural conditions on sandy gravels; (**f**) Saturation conditions on sandy gravels.

For each gravel, the shear strength parameters under saturated conditions are less than those under natural conditions. For fine-grained muddy gravels, especially, cohesion c′ is reduced by approximately 60%. Furthermore, for sandy gravels, internal friction angle f′ is reduced by approximately 28%. By comparing the broken gravels with the fine-grained muddy gravels with good early cementation, it can be seen that the gravel content of the former is about 8% higher on average, but the fine grain content is 7% less, as shown in Table 1. Under natural conditions, the f′ value is generally equivalent, and the c′ value of the former is 65% of the latter. In addition, the parameters of the two are basically the same under saturated conditions. By comparing the broken gravels with the sandy gravels, their

c' values are almost the same under the two conditions, while the f' value of sandy gravels is smaller than that of broken gravels.

Table 1. The strength parameters of field tests under natural and saturated conditions.

Parameters	Broken Gravels		Fine-Grain Muddy Gravels		Sandy Gravels	
	Natural Condition	Saturated Condition	Natural Condition	Saturated Condition	Natural Condition	Saturated Condition
c' (kPa)	49	35	76	36	49	36
f' (°)	36.1	32.2	36.5	31.8	32.2	23.3
Gravel content	10%	-	3%	-	-	-
Fine grain content	2%	-	10%	-	-	-

Laboratory tests for comparison were conducted using remolded soil samples because it was difficult to obtain the undisturbed samples of coarse-grained soil. The samples for laboratory tests were made of materials taken in the field after rubbles larger than 60 mm were sieved out. Density measurements were performed to control the densities of samples made in the laboratory and to ensure that the moisture contents of samples were close to those of natural deposits. Quick direct shear tests were conducted using samples with a diameter of 500 mm and a height of 300 mm. The shear strength parameters determined by laboratory tests are listed in Table 2.

Table 2. The strength parameters of laboratory shear tests under natural conditions.

Parameters	Broken Gravels	Fine-Grain Muddy Gravels	Sandy Gravels	Terrace Deposits	Early Debris Flow Deposits
c' (kPa)	44	59	39	38	49
f' (°)	35.8	35.3	30.5	36.5	31.4

By comparing the field test results with the laboratory test results in Tables 1 and 2, it can be seen that the values from laboratory tests are close to those from field tests, thus, the results of these two types of tests are mutually verifying. However, most values from laboratory tests are slightly smaller than those from field tests, and the c' values of fine-grained muddy gravels determined by laboratory tests are apparently smaller than those determined by field tests, except for the early debris flow deposits. This is because the large particles in the remolded soil samples are removed, and the relatively stable structure formed by the deposit under long-term accumulation is destroyed.

3.1.3. Stability Analysis

(a)　Stability analysis of the deposits before reservoir impoundment

Figure 5 presents a sectional view of the typical rock and soil structure of RS colluvial-deluvial deposits. The Rongsong deposit (RS) photos in Figure 3 are in correspondence with the profile of the numerical model in Figure 5. A computational analysis was performed using the Slide software from RocScience company. The Slide software is used to analyze the stability and failure mode of the deposits using the rigid body limit equilibrium method and the finite element strength reduction method based on the Mohr-Coulomb criterion. The bedrock is considered to have infinite strength, and each overburden layer is considered as homogeneous isotropic material. Therefore, the boundary on both sides of the numerical model is considered as horizontal constraint, and the bottom boundary is considered as fixed constraint. The 6-node triangular isoparametric element under plane strain condition is used for mesh generation. Herein, the f' values from field tests are used in the model, and the c' values used in the model are equal to 0.7 times the values from laboratory tests. The results show that the stability of the colluvial-deluvial deposit varies at different sliding surfaces, as shown in Figure 5b. For the mode of general slip with the boundary between

bedrock and overburden as the bottom slip plane, the stability factor is 1.30. For the mode of central slip with a poorly cemented broken gravel layer as the bottom slip plane, the stability factor is 1.27. For automatically searched circular slip, the minimum stability factor is 1.16, which occurs in the shallow surface layers of recent colluvial-deluvial deposits.
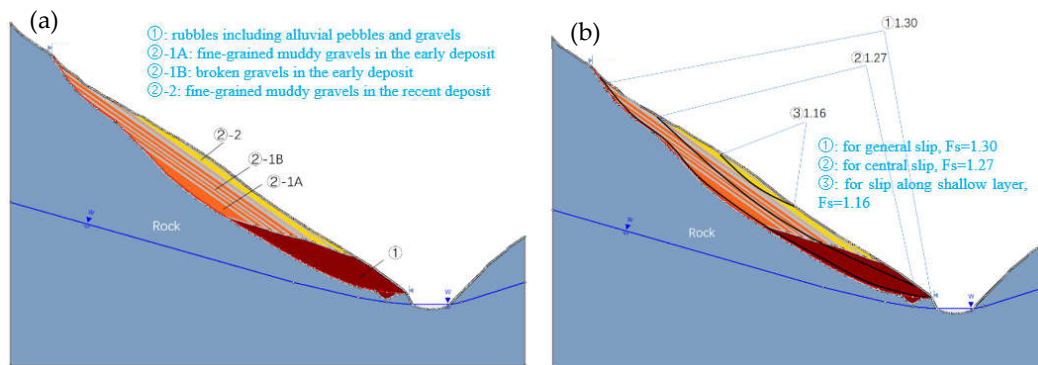

Figure 5. Numerical calculation results of the RS deposits in the high and cold valley: (**a**) Numerical model of the deposits; (**b**) Stability results of the RS deposit.

The reasons for the difference in the stability of the deposits in the high and cold valleys in different sliding surfaces are as follows. Firstly, there is little clay and vegetation on the original slopes on both sides of high and cold valleys. Moreover, weak clay layers or humus layers with good continuity are rarely seen in the bottom sections of colluvial-deluvial deposits, which is difficult to form a sliding surface. Therefore, the stability of the deposits is relatively good in general, such as the stability of the sliding surface ① in Figure 5b. According to the field investigations on more than 20 deposits in the upper reaches of the Lancang River, there is no large deformation or landslide under natural conditions. Secondly, the deposits in the middle and upper part of the slope are formed by multiple accumulations. The fine gravelly soil gravels with more fine-grained soil and the crushed gravel layers with less fine-grained soil are distributed alternately, forming an obvious rhythm. At the same time, their shear strength is also different. The c' value of the latter is lower than that of the former. The slope of the slope surface in the upper part is close to the natural angle of repose of crushed gravel. The cementation of these soil layers is weak and their stability is relatively low.

(b)   Stability analysis of the deposits after reservoir impoundment

Taking the RS deposit as an example, Figure 6 presents a sectional view of the typical rock and soil structure of the deposit. A computational analysis of the stability was performed using the Slide software from RocScience company, and finite element numerical simulation calculation of the deposit was conducted using the Phase2 software. The stability of the deposit is presented in Figure 6a. For the mode of general slip with the boundary between bedrock and overburden as the bottom slip plane, the stability factor is 1.07. For the mode of central slip with a poorly cemented broken gravel layer as the bottom slip plane, the stability factor is 1.05. For automatically searched circular slip, the minimum stability factor is 1.03. Therefore, most sections of the deposit are unstable, and the stability becomes lower and lower from the inside to the surface of the slope. After reservoir impoundment, the main form of the deformation of the deposit is progressive creep deformation from the surface to the inside. The results of finite element numerical simulation calculation are shown in Figure 6b,c. The maximum displacement occurs in the shallow surface. The shallow and middle weakly cemented gravel layer and the boundary plane between bedrock and overburden are the main areas of the shear deformation and failure of the accumulation.
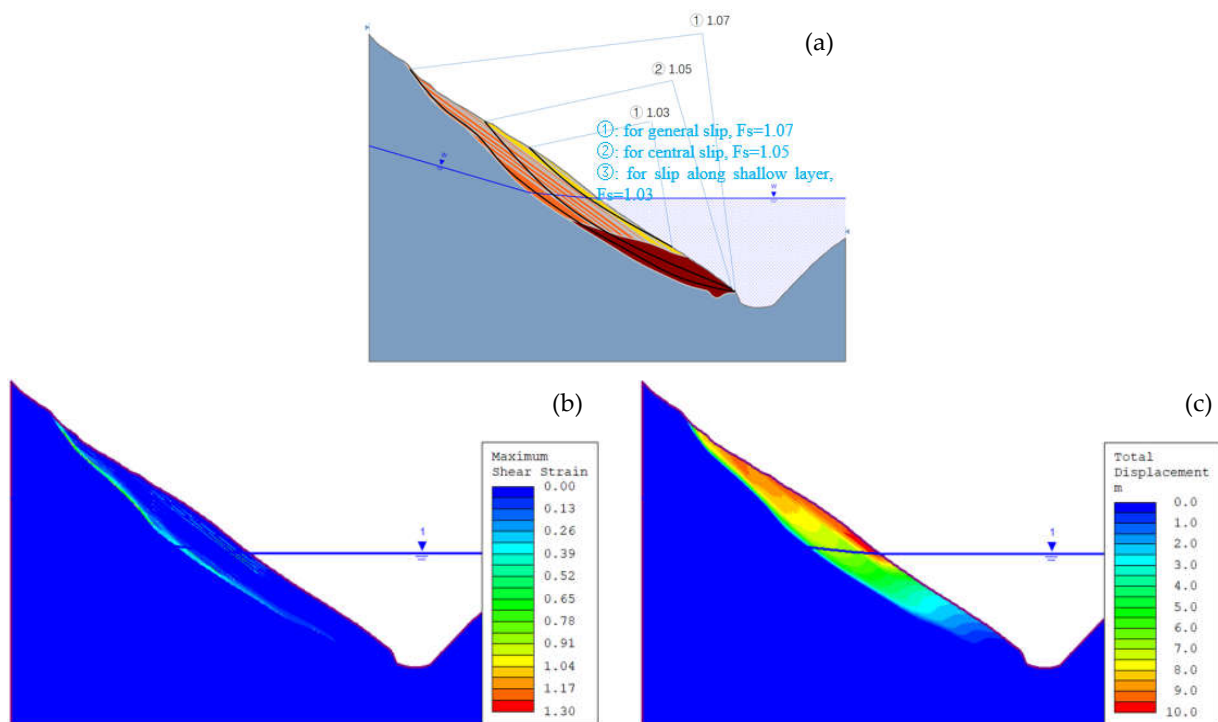
Figure 6. Numerical simulation results of the RS colluvial-deluvial deposits: (**a**) Stability; (**b**) Maximum shear strain; (**c**) Total displacement.

3.2. Terrace Deposits

3.2.1. Characteristics of Deposits

Terrace deposits are usually distributed in a belt-shaped pattern. However, in the high and cold valley regions, the terrace deposits are intermittently distributed, and many relatively independent and concentrated terrace deposits have been formed, as shown in Figure 7a. The reason is that the slopes in this region are generally steep and have been cut by many gullies, and few early fluvial deposits have been preserved. A near-parallel sedimentary rhythm can be observed in these deposits, as shown in Figure 7b. Compared with the terrace deposits in warm and humid regions at low altitudes, those in the high and cold valley regions have more special characteristics in terms of rock-soil structure as described below.

(a) There are many colluvial deposits on both banks of the riverbed in Figure 7c. In addition to sand gravel, there are a large number of rubble or gravel mixed in the riverbed deposits;

(b) As a terrace deposit, colluvial-deluvial gravelly soil accumulates on the riverbed deposits in the later period, forming a typical binary structure, as shown in Figure 7d.

3.2.2. Physical and Mechanical Properties

The samples of terrace deposits were from the RS deposit, No.7 deposit, No.4 terrace deposit in the RM Hydropower Station area. For pebbles and gravels in the terrace deposits, the test under the natural condition was conducted at 29–39 m of No.5 drift in the RS deposit, while the test under the saturated condition was conducted in the lower section of the No.7 deposit. Figure 8 presents the σ-τ scatter diagrams for field tests in pebbles and gravels in the terrace deposits. The results reveal that the shear strength parameters c′ and f′ are 37 kPa and 36.9° under natural conditions, respectively. Meanwhile, they are 33 kPa and 32.2° under saturated conditions, respectively.
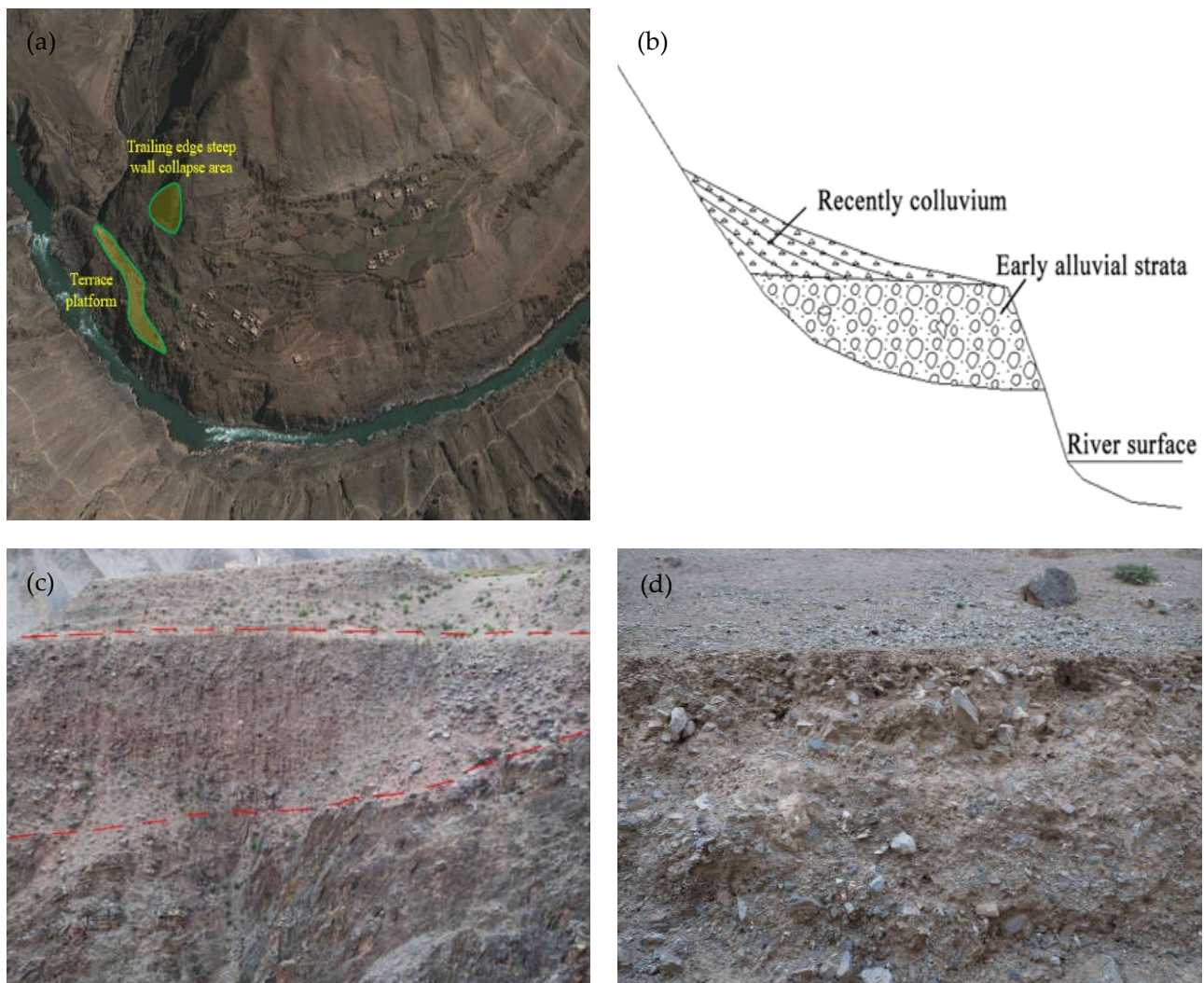
Figure 7. Terrace deposits in the high and cold valley: (**a**) Remote sensing image; (**b**) Typical binary structure; (**c**) riverbed deposits; (**d**) colluvial-deluvial gravelly soil.
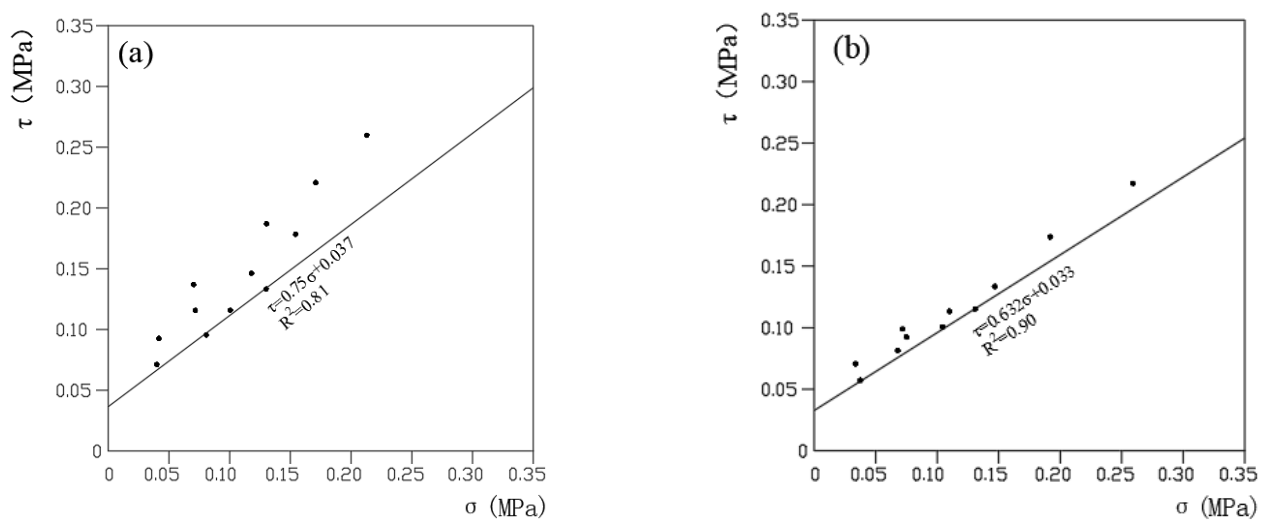

Figure 8. σ-τ scatter diagrams for field tests on pebbles and gravels in terrace deposits: (**a**) Natural conditions; (**b**) Saturation conditions.

3.2.3. Stability Analysis

(a)   Stability analysis of the deposits before reservoir impoundment

Figure 9 presents a sectional view of the typical rock and soil structure of terrace deposits. The terrace deposit photos in Figure 7 are in correspondence with the profile of the numerical model in Figure 9. The No.4 terrace deposit is mainly composed of sand, pebble, and gravel, and the terrain is generally flat. A computational analysis of the No.4 terrace deposit was performed using the Slide software from RocScience company. For the mode of general slip with the boundary between bedrock and overburden as the bottom slip plane, the stability factor is 3.74. For automatically searched circular slip, the minimum stability factor is 1.08.
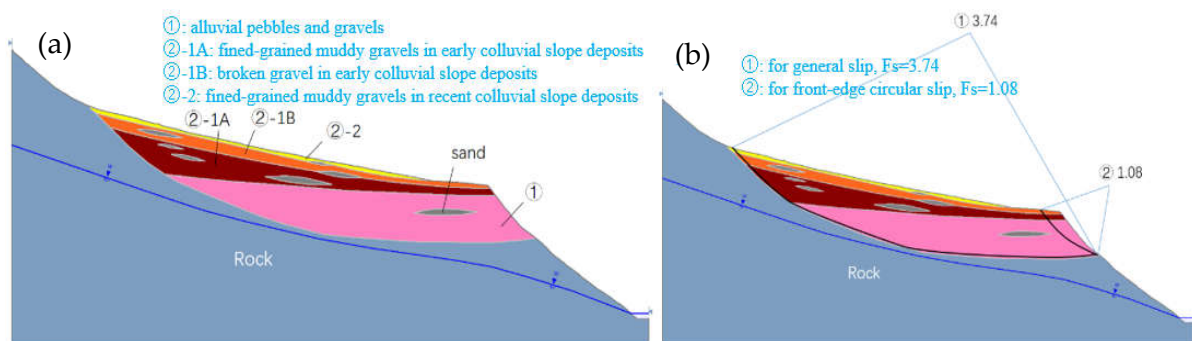

Figure 9. Numerical calculation results of the No.4 terrace deposits in the high and cold valley: (**a**) Numerical model of the deposits; (**b**) Stability results of the No.4 deposit.

The reasons for the difference in the stability of the deposits in the high and cold valleys in different sliding surfaces are as follows. Firstly, in addition to sand, pebble, and gravel, there are also toppling and river-blocking materials in the riverbed deposits of high and cold valleys, which change the local stability of terrace deposits. Secondly, the upper part of the terrace deposit will generally accumulate a certain thickness of late colluvial-deluvial deposits, which belongs to the upper loading, and will reduce the stability of the terrace deposit. When there are too many colluvial-deluvial deposits in the upper part, the stability of the terrace deposit is controlled by colluvial-deluvial deposits, and the stability factor of the terrace deposit will be significantly reduced. Finally, the valley has a strong undercutting effect and less rainfall in the later period. The leading edge of the terrace deposit is high and steep, with poor stability. Therefore, the terrace deposit may collapse and slide locally.

(b)   Stability analysis of the deposits after reservoir impoundment

Taking the No.4 deposit as an example, Figure 10 presents a sectional view of the typical rock and soil structure of the deposit and its stability results. For the mode of general slip with the boundary between bedrock and overburden as the bottom slip plane, the stability factor is 3.19. Therefore, after the reservoir impoundment, the deposit below the reservoir water will experience the uplift pressure of the water, and the soil parameters will also be reduced to a certain extent. However, the bottom interface of the deposit is gentle, and the slope surface is gentle. Therefore, the overall stability of the deposit is still good. For automatically searched circular slip, the minimum stability factor is 1.00. In this case, the stability of the deposit is obviously poor. The deformation and failure of the deposit mainly occur on the steep slope near the river at the leading edge of the terrace, as shown in Figure 10b,c. The deformation and failure mode of the deposit is mainly bank collapse at the leading edge.
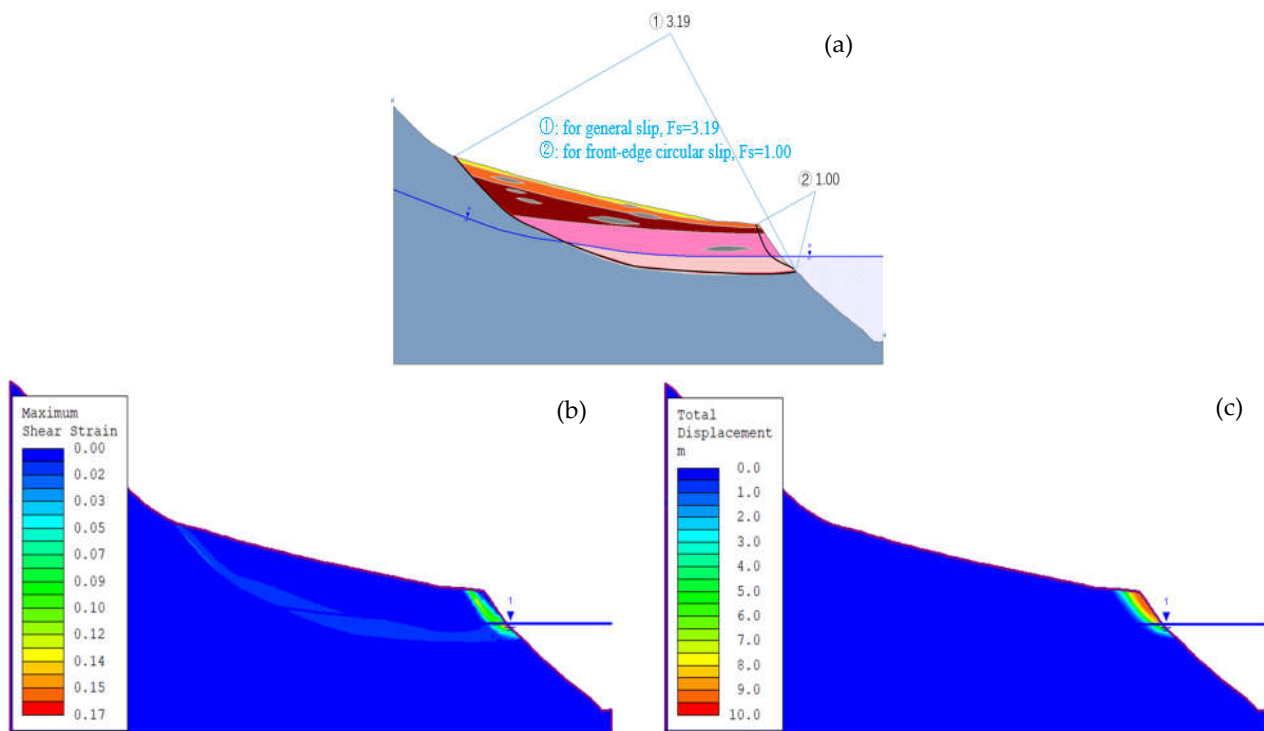
Figure 10. Numerical simulation results of terrace deposits: (**a**) Stability; (**b**) Maximum shear strain; (**c**) Total displacement.

3.3. Early Debris Flow Deposits

3.3.1. Characteristics of Deposits

The early debris flow deposits are generally higher than modern gullies due to their early formation time. They are not affected by the existing river water and debris flow and are well-cemented. Compared with the debris flow deposits in warm and humid regions at low altitudes, those in the high and cold valley regions have more special characteristics in terms of rock-soil structure as described below.

(a) Debris flow gullies have been developed pervasively. According to the investigation results, among the 51 gullies along the Lancang River section from Mangkang County to Chaya County, there are 15 debris flow gullies, accounting for 29% of the total number of gullies. The reasons can be summarized by the following two aspects. The first is that the upper crust in this region is in the rapid uplift stage. The gullies on both sides of the valleys are steep in general, which creates favorable terrain conditions for the occurrence of debris flows. The second is that broken surface rocks, collapse, dislocation, landslide, and other adverse geological phenomena are developed, providing a rich source of solid materials for the formation of debris flow.

(b) Most debris flow deposits have a large scale. The reasons can be summarized by the following two aspects. The first is that the early glacial deposits from gullies and large-scale slumps provide the necessary source conditions for debris flows. For example, three deposits have been developed on the riverbanks of the Jinsha River near Wangdalong (WDL) Village downstream of Batang County in Sichuan Province, as shown in Figure 11a. The quantity of each deposit is more than 0.1 billion m^3. On the right bank of the Lancang River section in RM County of Tibet, No. 12 debris flow deposit is distributed along the riverbank over a distance of 1.4 km and has a maximum width of 0.8 km. The debris flow deposit is fan-shaped and covers the second terrace. Apparently, large-scale slumps have occurred in the source gully, as shown in Figure 11b–d. This large debris flow deposit has even blocked the Lancang River and resulted in the displacement of the river channel to the left. The second is that the melting of ice and snow and glacial lake outburst caused by climate

changes provide an adequate water supply for ultra-large-scale debris flows. From the perspective of the deposit-terrace, the WDL and No.12 debris flow deposits have all covered the second terrace, but they have not fully covered the first terrace, indicating that these deposits were formed in the same geological period as the first terrace. The formation geological period of the two deposits is the early Holocene. This phenomenon is highly consistent with the rapid warming during the early-middle Holocene after the Last Glacial Maximum in the southeast of Tibet [29].
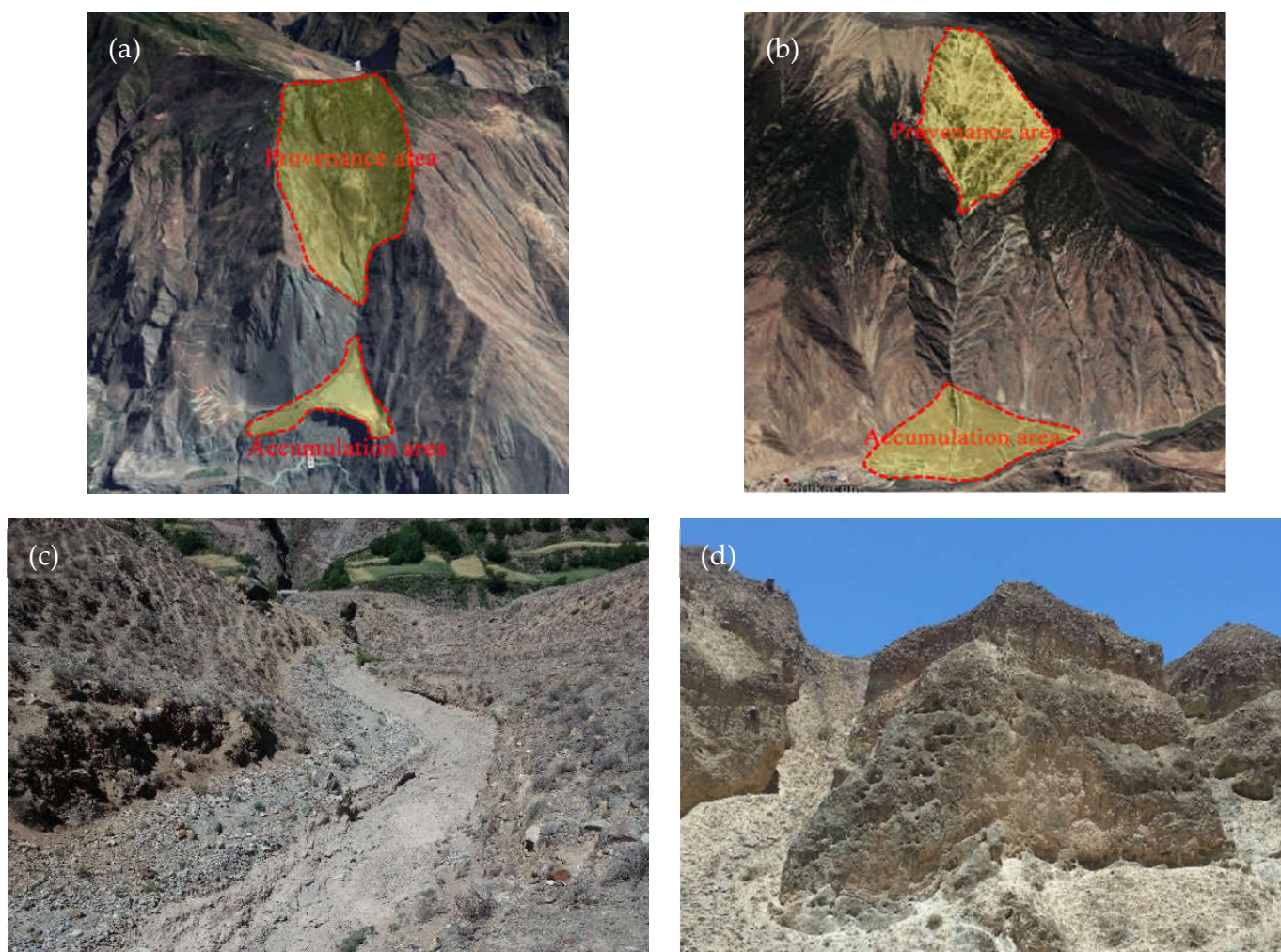
Figure 11. Early debris flow deposits in the high and cold valleys: (**a**) Remote sensing image of early WDL deposit; (**b**) Remote sensing image of No.12 deposit; (**c**) No.12 deposit in the RM Hydropower Station area; (**d**) The scarps and caves formed by weathering of No.12 deposits.

3.3.2. Physical and Mechanical Properties

The samples of debris flow deposits were from the No.12 deposit in the RM Hydropower Station area. Figure 12 presents the σ-τ scatter diagrams for field tests in sandy gravels in debris flow deposits. The results reveal that the shear strength parameters c′ and f′ are 32 kPa and 32.2° under natural conditions, respectively. Meanwhile, they are 28 kPa and 24.7° under saturated conditions, respectively.
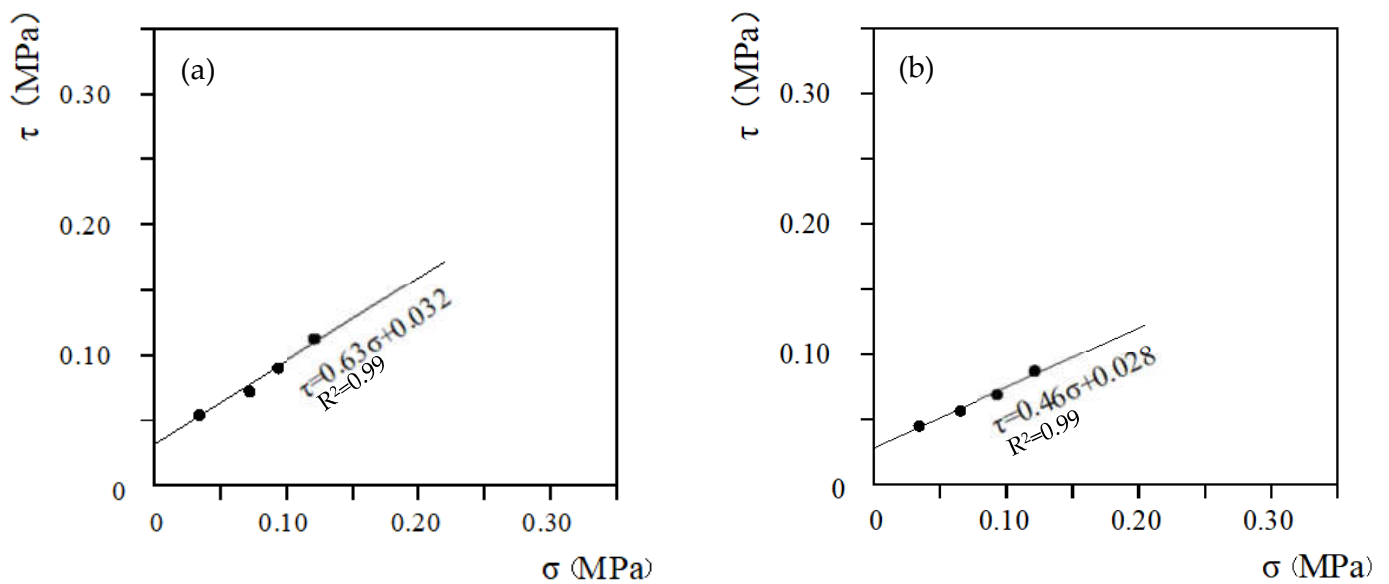
Figure 12. σ-τ scatter diagrams for field tests on sandy gravels in debris flow deposits: (**a**) Natural conditions; (**b**) Saturation conditions.

3.3.3. Stability Analysis

(a) Stability analysis of the deposits before reservoir impoundment

Taking the No.12 debris flow deposit as an example, Figure 13 presents a sectional view of the typical rock and soil structure of the deposit and its stability results. The debris flow deposit photos in Figure 11 are in correspondence with the profile of the numerical model in Figure 13. For the mode of general slip with the boundary between bedrock and overburden as the bottom slip plane, the stability factor is 1.81. For automatically searched circular slip, the range of the stability factor is 1.53–1.55. Therefore, the overall stability of the deposit is still good.
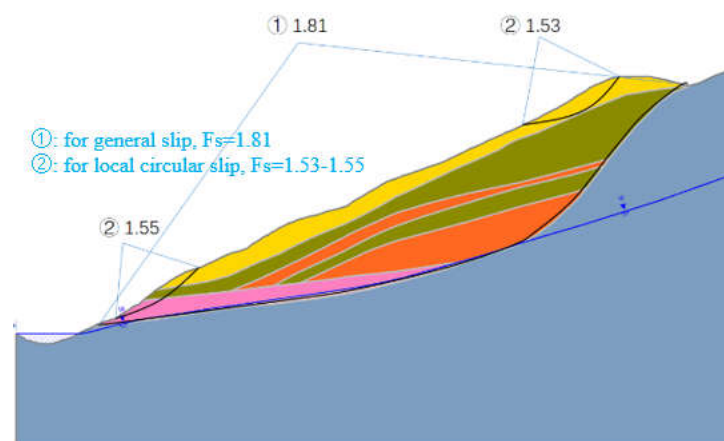

Figure 13. Stability results of the No.12 debris flow deposits in the high and cold valley.

(b) Stability analysis of the deposits after reservoir impoundment

Figure 13 presents the stability results and the deformation characteristics of the No.12 debris flow deposit at RM Hydropower Station. The early debris flow deposit is mainly composed of crushed gravel, and the terrain is generally gentle. For the mode of general slip with the boundary between bedrock and overburden as the bottom slip plane, the stability factor is 1.55. For automatically searched circular slip, the stability factor is 1.31. The deposit is in a stable state under natural conditions. After impoundment, the deposit

below the reservoir water will be affected by the uplift pressure of the water, and the soil parameters will also be reduced to a certain extent. However, the stability of the deposit is still good on the whole due to the gentle bottom interface and slope surface. Figure 14b,c reveal that the deformation and failure of the deposit mainly occur in steep local areas.
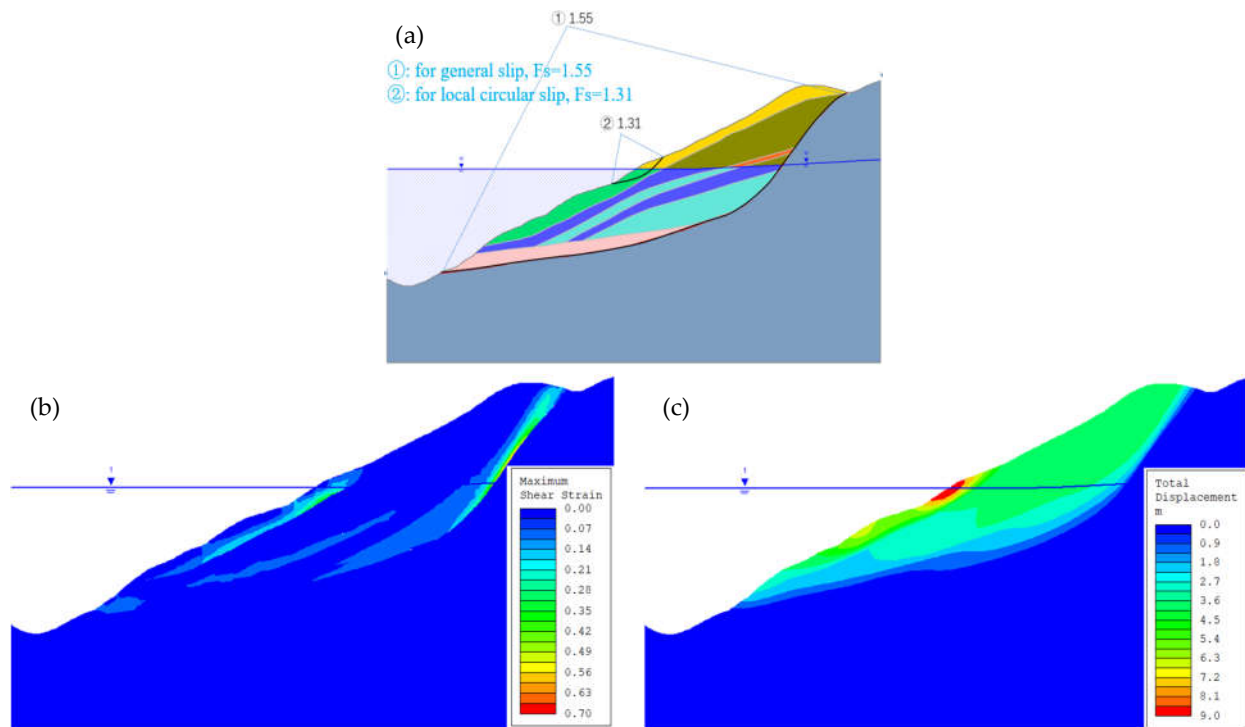

Figure 14. Numerical simulation results of debris flow deposits: (**a**) Stability; (**b**) Maximum shear strain; (**c**) Total displacement.

3.4. Landside Deposits

3.4.1. Characteristics of Deposits

Compared with the landslide deposits in warm and humid regions at low altitudes, those in the high and cold valley regions have two special characteristics in terms of rock-soil structure as described below.

(a) The bedrock is strongly compressed by the structure, the surface is weathered and unloaded strongly, and earthquakes occur frequently. Therefore, large-scale landslides are common. For example, the No.1 deposit in front of the dam of CB hydropower station has a total volume of 27 million m^3, which is a slump deposit formed under early seismic actions. The deposit is composed of broken rock masses, including the broken granite and marble from the hanging wall of the Suwalon-Wangdalong Fault in the Jinsha River fault zone, as shown in Figure 15a. Large quantities of rubbles and huge blocks have blocked the Jinsha River, and damming silts have been deposited in the upper reaches of the river. Afterwards, the deposit was flushed and divided by the river water into two parts on both riverbanks. However, large-scale landslides have also occurred recently. For example, the Baige Landslide, which occurred on the right bank of the Jinsha River in BL Town of JD County in October 2018, has formed an ultra-large-scale landslide deposit with a length of about 1600 m, a maximum width of about 700 m, and a total volume of about 3500×10^4 m^3. This landslide deposit has even blocked the Jinsha River, as shown in Figure 15b. The formation mechanism of the deposit is due to the deformation and failure of the melange rock mass in the tectonic suture zone under the continuous action of unloading and gravity.
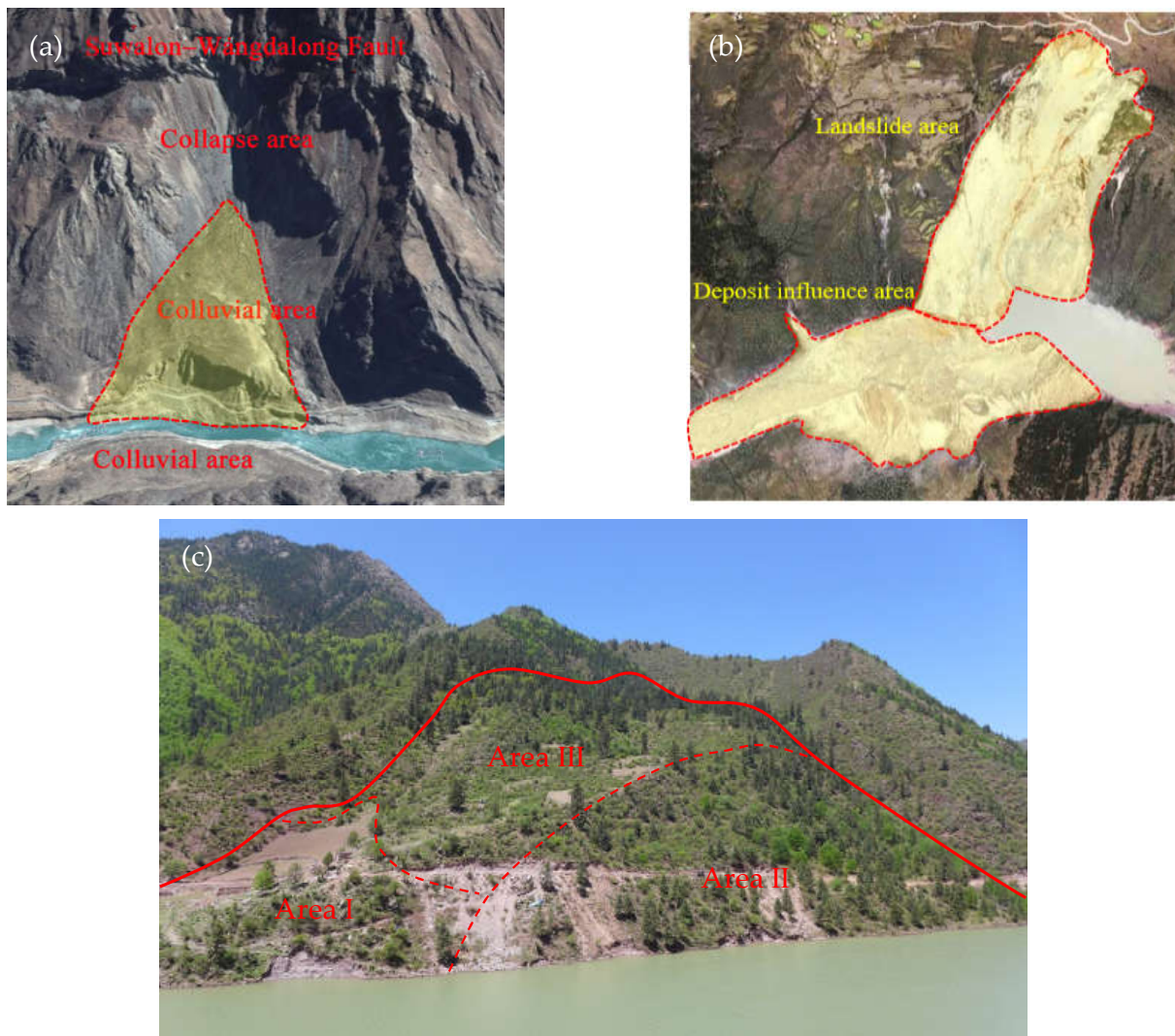
Figure 15. Landslide deposits in the high and cold valleys: (**a**) Remote sensing image of No.1 deposit; (**b**) Remote sensing image of the Baige landslide deposit; (**c**) Overall view of the Jiasai landslide deposit.

(b) Ice and snow meltwater are the main causes of large-scale landslides. The high and cold valley region is an area with low rainfall. For example, the average annual rainfall and maximum daily rainfall in the Lancang River valley in Mangkang area are 575 mm and 55 mm, respectively, accounting for only 1/2–1/3 of the average annual rainfall and maximum daily rainfall in inland areas. Therefore, it is difficult for the rainwater to seep into the rock and soil masses at deep levels to create deep underground flows or adequate fissure water pressure, as shown by the Jiasai landslide deposit in Figure 15c. Three deformation zones are divided into the Jiasai landslide deposit. The deformation of each zone is different because the permeability coefficient of the rock and soil is different. However, the probability of occurrence of large-scale landslides will increase significantly when ice and snow meltwater and storm water work together as the temperature rises during the period from April to October each year.

3.4.2. Stability Analysis

(a) Stability analysis of the deposits before reservoir impoundment

Under natural conditions, landslides in this study area can be classified into two major types including water-induced landslides and earthquake-induced landslides. The water-induced landslide is characterized by gradual development, slow starting, low sliding speed, and long evolution time. When the landslide reaches a new balance, the landslide stops moving and tends to stabilize to form an old landslide or an ancient landslide. The stability of the landslide is not high, and mostly in a basically stable-unstable state. When the external conditions change slightly, the landslide is very easy to revive. For example, based on the analysis of the Jiasai landslide deposit that has been deformed after the impoundment of GD Hydropower Station, its stability factor under natural conditions is only 1.05–1.07, as shown in Figure 16. The landslide deposit photos in Figure 15 are in correspondence with the profile of the numerical model in Figure 16. The earthquake-induced landslide has the characteristics of fast starting, short evolution time, high sliding speed, etc. This kind of old landslide or ancient landslide has a relatively low and gentle terrain, a relatively flat slope surface, and high stability. The possibility of such landslide revival is small.
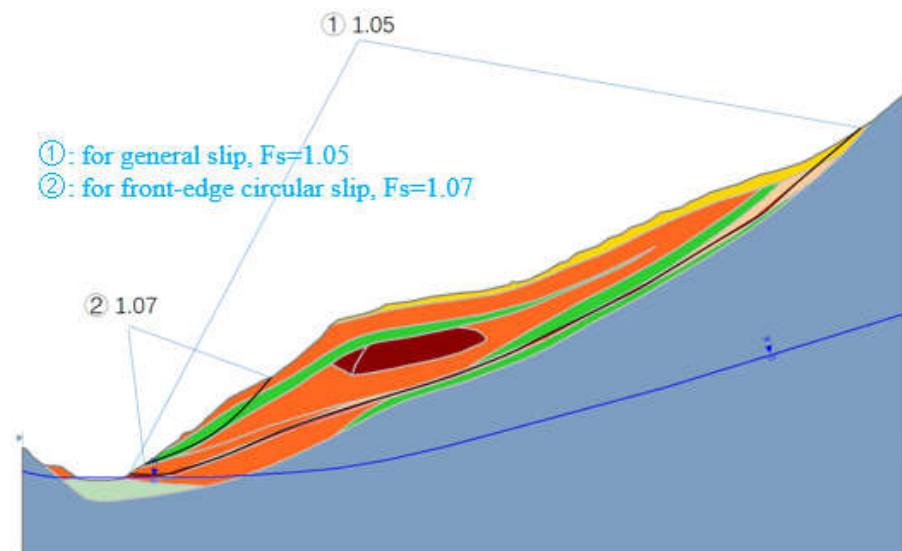

Figure 16. Stability results of the Jiasai landslide deposits in the high and cold valley.

(b)   Stability analysis of the deposits after reservoir impoundment

Taking the Jiasai landslide deposit at GD Hydropower Station as an example, the deformation characteristics of the deposit after the impoundment are as follows. Firstly, according to the remote sensing image before the impoundment, the Jiasai landslide is an old landslide with an obvious chair shape, as shown in Figure 17a. Secondly, the exploration results show that the Jiasai landslide is mainly composed of rubble, and there are layered giant blocks with a length of more than ten meters to tens of meters. However, there is a through weak soil layer mainly composed of gravelly clay in the middle and lower part of the landslide, as shown in Figure 17c. Finally, field investigation shows that after one month of the reservoir impoundment, tension cracks are found in the leading edge of the middle and upstream sides. About two months later, tension cracks are also found in the back scarp of the landslide. After about four months of impoundment, the tension cracks have connected the width of the cracks is 30–100 cm. Moreover, the trailing edge of the landslide is staggered about 1–1.5 m, as shown in Figure 17c,d. Surface deformation monitoring is shown in Figure 17e.
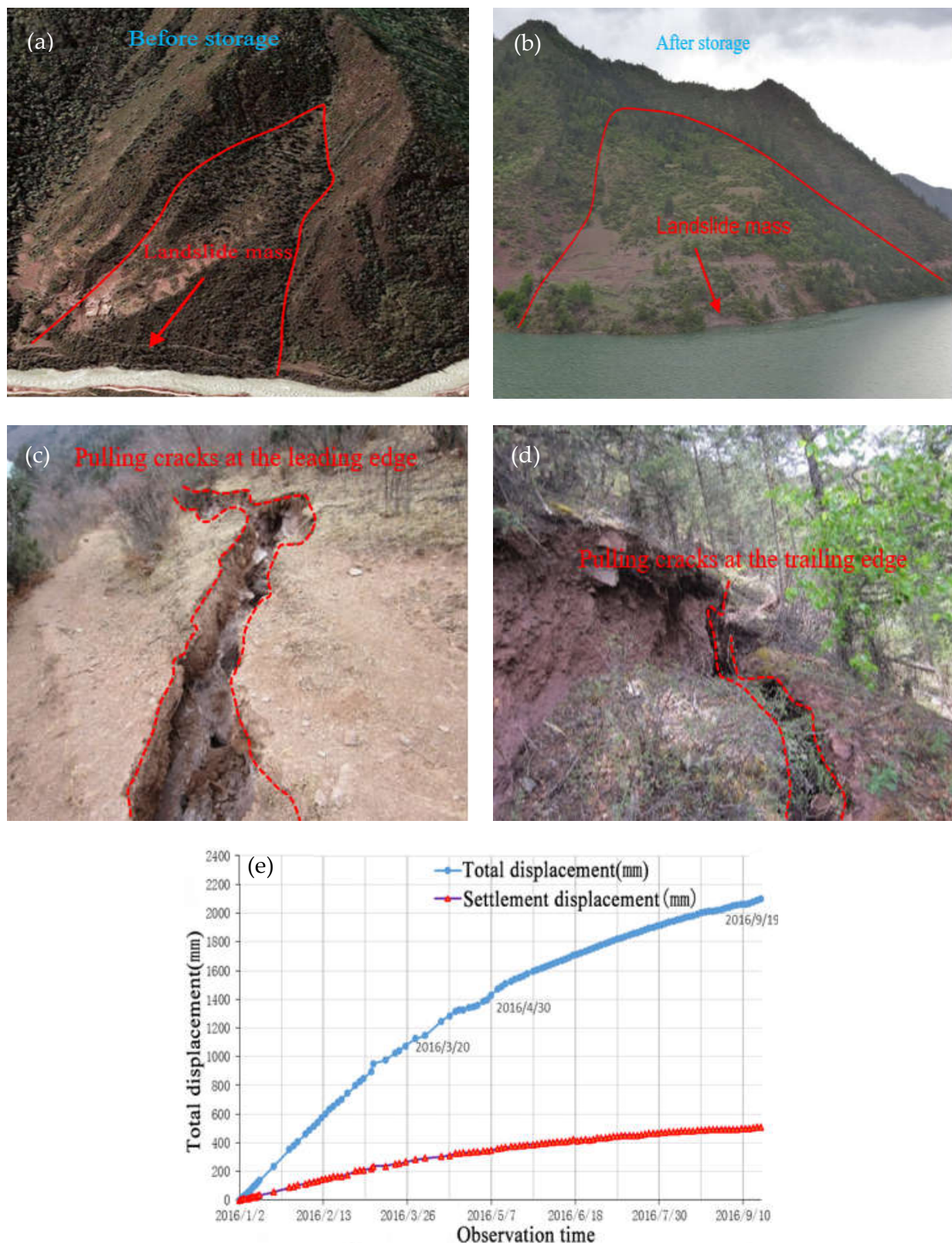
Figure 17. Deformation characteristics and monitoring curves of the Jiasai landslide deposits after the reservoir impoundment: (**a**) Remote sensing image before the impoundment; (**b**) Overall view after the impoundment; (**c**) Tension cracks at the head scarp; (**d**) Tension cracks at the back scarp; (**e**) Time-surface displacement curves.

Figure 18 presents the finite element results of the Jiasai deposit at GD Hydropower Station. It can be seen from the figure that the shear stress concentration area of the landslide after the impoundment is mainly distributed in the leading edge and the lower weak interlayer, which is in good agreement with the formation of tension cracks observed on the leading edge and the trailing edge on site. The numerical simulation results and the field monitoring results show that there are two main deformation and failure modes of a landslide after impoundment. First, bank collapse occurs at the front steep slope. The second is the overall sliding along the early bottom slip surface or the internal penetrating soft layer. Compared with displacement data from some data points in the simulation model and the data obtained in-situ, at the trailing edge of the landslide, the actual deformation of the landslide is consistent with that of the numerical model. On the whole, its deformation is relatively large, which is related to the impoundment of the reservoir. The rapid rise of the reservoir water level has formed the stress condition of the landslide that is not conducive to stability and formed the mechanical model of "pushing up and supporting down" to induce the landslide. The soft intercalated sliding zone soil is saturated, resulting in the reduction of shear strength. The water level of the leading-edge reservoir rises rapidly to form buoyancy. The rainwater at the leading edge fills the cracks and seeps along the cracks, generating hydrostatic pressure in the cracks and uplift pressure on the sliding zone. This will reduce the anti-sliding force and increase the sliding force.
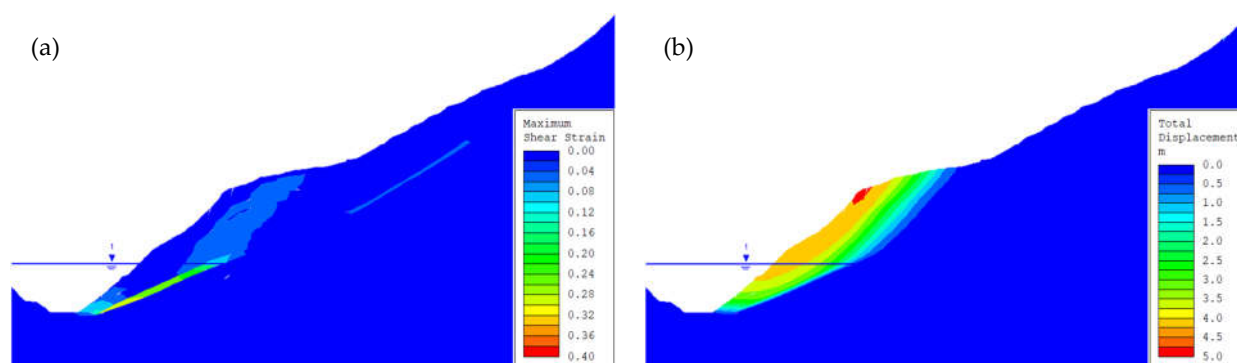

Figure 18. Numerical simulation results of landslide deposits: (**a**) Maximum shear strain; (**b**) Total displacement.

4. Discussion

The construction of the hydropower station can develop and utilize water resources and improve the water environment in the alpine valley. However, the reservoir impoundment will also change some original geological bodies and bring new challenges to the project construction. The impact of the reservoir impoundment on the stability of bank slope deposits in the high and cold valleys is mainly shown in the following three aspects.

(a) The uplift pressure of the water is unfavorable to the stability of the deposits. When the reservoir water rises, the surface and groundwater levels inside the deposits will be raised as a whole, so that the deposits are partially under the constant water level. This will form the uplift pressure to reduce the weight of the lower sliding bodies, thus reducing the stability of the deposits. As shown in Figures 5b and 19, compared with the stability analysis of the deposits before reservoir impoundment, when the shear strength remains unchanged and only the unit weight of soil mass below the water level is converted to saturated unit weight, the stability factor of the RS colluvial-deluvial deposit decreases from 1.30 to 1.19. Compared with the stability analysis of the deposits after reservoir impoundment, the stability factor of the RS colluvial-deluvial deposit increases from 1.19 to 1.07, as shown in Figures 6a and 19. For calculation of the result of the stability of the RS deposit after the impoundment in Figure 19, only the uplift pressure of the water is considered. Therefore, the stability factor is larger than that in the calculation result in Figure 6. The reason is that for

calculating the result of the stability of the RS deposit after the impoundment in Figure 6, the uplift pressure, seepage pressure, hydrostatic pressure and hydrodynamic pressure of the water are considered. These factors cause the anti-sliding force to decrease and the sliding force to increase. The influence factors of the deposits are often realized through the change of groundwater, which will significantly change the stress conditions of the deposits and the physical and mechanical properties of rock and soil mass, thereby reducing the stability of the deposits. The rapid rise of the groundwater level caused by the rise of the reservoir water level will form a large hydrostatic pressure on the potential slip surface. The sliding body at the leading edge of the anti-slide section is submerged by the reservoir water, resulting in an increase in the uplift pressure, while the effective normal stress will be reduced, reducing the anti-slide force at the anti-slide section.
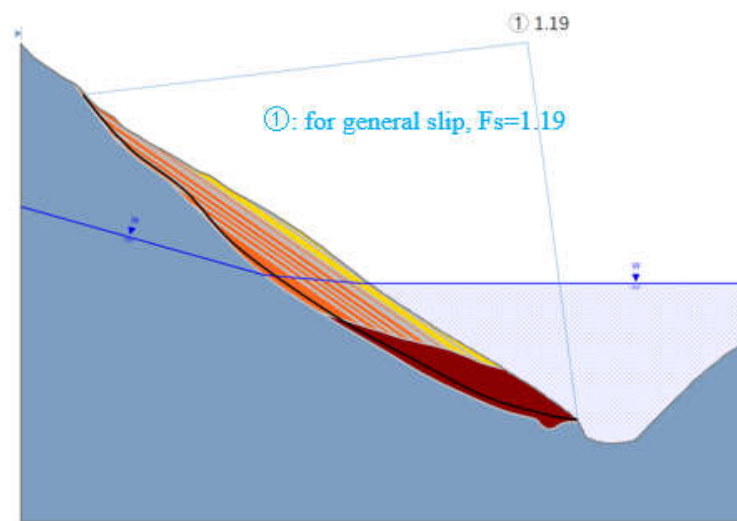

Figure 19. Calculation result of the stability of the RS deposit after the impoundment (only the uplift pressure of the water is considered).

(b) The mechanical properties of soil mass decrease. Microstructure tests of fine particles such as clay and silt show that water immersion will cause slip and tensile deformation between soil particles. Subsequently, the particles are also broken and corroded. These factors reduce the particle size and increase the pore spacing. Therefore, the microstructure of soil mass will be destroyed, and the mechanical properties of the soil will be reduced, especially the cohesion of soil. For coarse particles such as pebbles and gravels, water will reduce the friction between particles, and the friction of soil. The shear strength of the soil will decrease, reducing the stability of the deposit. Therefore, fine-particle soil is more hydrophilic than coarse-particle soil, and the wetting effect of water of the former is stronger. For example, compared with the natural conditions, the f' value of fine particle soil under saturated conditions decreases by 16%, and the c' value decreases by 53%. Nevertheless, the f' value of coarse particle soil decreases by 14%, and the c' value decreases by 29%, as shown in Table 1.

(c) The seepage pressure of the water is unfavorable to the stability of the deposits. When the reservoir water drops rapidly, the residual groundwater in the soil will seep out, and the seepage pressure will be formed. Finally, the force causing soil deformation is increased, and the stability of the deposit is reduced.

In general, the water impoundment will deteriorate the geological conditions of the deposits of the river valley and reduce the stability of the deposits. However, the influence of the impoundment on the deposit with different genesis and material compositions is different. The colluvial-deluvial deposit is less affected by water during its formation.

However, after the impoundment, the external environment of the deposit will change substantially, and the mechanical parameters and stability conditions of the soil will also decrease significantly, which is unfavorable to the stability of the deposit. Terrace deposit and debris flow deposit can only be formed under the condition of the water. The material composition, accumulation structure and shape of the deposits are often affected by the water. Therefore, the deterioration effect of the reservoir impoundment on the deposit is weaker than that of colluvial-deluvial deposit. After the reservoir impoundment, the deformation of the landslide increases significantly and is greatly affected by water.

The stability factor of the deposits can be calculated by finite element numerical simulation, which provides reference for the evaluation of landslide. When the calculated safety factor is small, reinforcement measures are needed for the deposits. At this point, different anchoring methods can be planned according to the potential sliding surface in numerical simulation. For large deformation area of the deposits, the number of anchor cable rows can be increased appropriately. In addition, support structure can be calculated by finite element method, such as checking thrust on antislide pile, calculating internal force of antislide pile and optimizing design of structure.

5. Conclusions

This paper presented a preliminary study on the special characteristics, formation mechanism, and stability analysis of four types of the deposits and the physical and mechanical properties of soil mass under natural and saturated conditions on the high and cold valleys in the Qinghai-Tibet Plateau. The following conclusions were drawn about the colluvial-deluvial deposit, the terrace deposit, the debris flow deposit, and the landslide deposit.

(a) The colluvial-deluvial deposits in high and cold valleys are widely distributed on both banks of the river, with the characteristics of large burial depth and large volume. The formation mechanism of the deposit is mainly related to the alternating action of weathering, rainfall, freezing–thawing, and earthquake triggering, so the rock mass produces large deformation. The colluvial-deluvial deposits in the high and cold valley regions have special characteristics. Firstly, the high and cold valley region is characterized by high regional in-situ stress, strong unloading, freezing–thawing, and weathering effects. Secondly, under tectonic and seismic actions, the rock masses are fractured noticeably and have many small and hidden joints. Finally, the layer in the RS deposit mainly includes a well cemented and fine-grained muddy gravel layer with high silt and clay content, and a poorly cemented broken gravel layer with low silt and clay content. For each gravel, the shear strength parameters under saturated conditions are less than those under natural conditions. After reservoir impoundment, the deposit is stable. However, after the reservoir impoundment, the deposit is unstable, and the main form of the deformation of the deposit is progressive creep deformation from the surface to the inside.

(b) The terrace deposits in the high and cold valley region are intermittently distributed, and many relatively independent and concentrated terrace deposits have been formed. The test results reveal that the shear strength parameters c' and f' are 37 kPa and 36.9° under natural conditions, while 33 kPa and 32.2° under saturated conditions. For the mode of general slip with the boundary between bedrock and overburden as the bottom slip plane, the stability factor of the deposit before the reservoir impoundment is 3.74, while is 3.19 after the reservoir impoundment. For automatically searched circular slip, the minimum stability factor is 1.08, while it is 1.00 after the reservoir impoundment. Therefore, the deformation and failure mode of the deposit is mainly the bank collapse at the leading edge.

(c) Debris flow gullies have been developed pervasively, and most debris flow deposits have a large scale. The test results reveal that the shear strength parameters c' and f' are 32 kPa and 32.2° under natural conditions, while they are 28 kPa and 24.7° under saturated conditions. For the mode of general slip with the boundary between bedrock

and overburden as the bottom slip plane, the stability factor of the deposit before the reservoir impoundment is 1.81, while it is 1.55 after the reservoir impoundment. For automatically searched circular slip, the range of the stability factor is 1.53–1.55, while the stability factor is 1.31 after the reservoir impoundment. Therefore, the deformation and failure of the deposit mainly occur in steep local areas.

(d) Due to the weathering of the surface, the unloading strongly, and earthquake frequently, large-scale landslide deposits in the high and cold valley region are common. The Jiasai landslide deposit has been deformed after the impoundment, and its stability factor under natural conditions is only 1.05–1.07. After one month of the reservoir impoundment, tension cracks in the Jiasai deposit are found in the leading edge of the middle and upstream sides. About two months later, tension cracks are also found in the back scarp of the landslide. After about four months of impoundment, the tension cracks have connected, and the width of the cracks is 30–100 cm. The results show that the bank collapse and overall sliding along the early bottom slip surface or the internal penetrating soft layer are the main deformation and failure modes of the landslide after impoundment.

References

1. Zhao, B.; Wang, Y.; Li, J.; Wang, J.; Tang, C. Insights into a giant landslide-prone area on the eastern margin of the Tibetan Plateau, China. *J. Mt. Sci.* **2021**, *18*, 21–37. [CrossRef]
2. Zhao, B.; Su, L.; Wang, Y.; Li, W.; Wang, L. Insights into some large-scale landslides along the Sichuan–Tibet railway, China. *J. Rock Mech. Geotech. Eng.* 2022, *in press*. [CrossRef]
3. Dortch, J.M.; Owen, L.A.; Haneberg, W.C.; Caffee, M.W.; Dietsch, C.; Kamp, U. Nature and timing of large landslides in the Himalaya and Transhimalaya of northern India. *Quat. Sci. Rev.* **2009**, *28*, 1037–1054. [CrossRef]
4. Zeng, Q.; Zhang, L.; Davies, T.; Yuan, G.; Xue, X.; Wei, R.; Yin, Q.; Liao, L. Morphology and inner structure of Luanshibao rock avalanche in Litang, China and its implications for long-runout mechanisms. *Eng. Geol.* **2019**, *260*, 105216. [CrossRef]
5. Ilinca, V. Using morphometrics to distinguish between debris flow, debris flood and flood (Southern Carpathians, Romania). *Catena* **2021**, *197*, 104982. [CrossRef]
6. Gao, R.; Wang, C.; Liang, Z. Comparison of different sampling strategies for debris flow susceptibility mapping: A case study using the centroids of the scarp area, flowing area and accumulation area of debris flow watersheds. *J. Mt. Sci.* **2021**, *18*, 1476–1488. [CrossRef]
7. Sun, X.; Chen, J.; Bao, Y.; Han, X.; Zhan, J.; Peng, W. Landslide Susceptibility Mapping Using Logistic Regression Analysis along the Jinsha River and Its Tributaries Close to Derong and Deqin County, Southwestern China. *ISPRS Int. J. Geo-Inf.* **2018**, *7*, 438. [CrossRef]
8. Guo, X.; Ge, Y.; Zhan, M.; Yan, H. Failure process of a lateral slope deposit and its effect on debris flood formation. *Bull. Eng. Geol. Environ.* **2022**, *81*, 324. [CrossRef]
9. Lin, J.; Zhu, G.; Wei, J.; Jiang, F.; Wang, M.; Huang, Y. Mulching effects on erosion from steep slopes and sediment particle size distributions of gully colluvial deposits. *Catena* **2018**, *160*, 57–67. [CrossRef]

10. Wen, T.; Tang, H.; Huang, L.; Wang, Y.; Ma, J. Energy evolution: A new perspective on the failure mechanism of purplish-red mudstones from the Three Gorges Reservoir area, China. *Eng. Geol.* **2020**, *264*, 105350. [CrossRef]

11. Fang, K.; Tang, H.; Li, C.; Su, X.; An, P.; Sun, S. Centrifuge modelling of landslides and landslide hazard mitigation: A review. *Geosci. Front.* **2023**, *14*, 101493. [CrossRef]

12. Liu, S.L.; Wang, L.Q.; Zhang, W.G.; He, Y.W.; Samui, P. A comprehensive review of machine learning-based methods in landslide susceptibility mapping. *Geol. J.* **2023**. [CrossRef]

13. Wang, L.Q.; Xiao, T.; Liu, S.L.; Zhang, W.G.; Yang, B.B.; Chen, L.C. Quantification of model uncertainty and variability for landslide displacement prediction based on Monte Carlo simulation. *Gondwana Res.* **2023**. [CrossRef]

14. Jiang, F.S.; Huang, Y.H.; Wang, M.K.; Lin, J.S.; Zhao, G.; Ge, H.L. Effects of Rainfall Intensity and Slope Gradient on Steep Colluvial Deposit Erosion in Southeast China. *Soil Sci. Soc. Am. J.* **2014**, *78*, 1741–1752. [CrossRef]

15. Wen, T.; Hu, Z.; Tang, H. The field survey and deformation characteristics of exit slope of Qingshuigou tunnel in the southwest of China. *Arab. J. Geosci.* **2022**, *15*, 1096. [CrossRef]

16. Jia, W.; Wen, T.; Li, D.; Guo, W.; Quan, Z.; Wang, Y.; Huang, D.; Hu, M. Landslide Displacement Prediction of Shuping Landslide Combining PSO and LSSVM Model. *Water* **2023**, *15*, 612. [CrossRef]

17. Zhang, W.G.; He, Y.W.; Wang, L.Q.; Liu, S.L.; Meng, X.Y. Landslide Susceptibility Mapping Using Random Forest and Extreme Gradient Boosting: A Case Study of Fengjie, Chongqing. *Geol. J.* **2023**. [CrossRef]

18. Jiang, F.; Huang, Y.; Wang, M.K.; Lin, J.; Zhao, G.; Ge, H.; Ji, X. Sediment selective behaviors of colluvial deposit materials on steep slopes and under heavy rainfall conditions in southeastern China. *J. Soil Water Conserv.* **2018**, *73*, 133. [CrossRef]

19. Zhang, Y.; Chen, N.; Liu, M.; Wang, T.; Deng, M.; Wu, K.; Khanal, B.R. Debris flows originating from colluvium deposits in hollow regions during a heavy storm process in Taining, southeastern China. *Landslides* **2020**, *17*, 335–347. [CrossRef]

20. Vandenberghe, J.; Vanacker, V. Towards a system approach in the study of river catchments. *Geomorphology* **2008**, *3*, 173–175. [CrossRef]

21. Wen, Z.; Chen, D.; Guo, L.; Pan, B.; Hu, X.; Li, Q.; Ji, X.; Yang, J. Response of terrace deposit thickness to climate change and tectonic deformation: An example of the Liyuan River in the Northeast Tibetan Plateau. *Terr. Nova* **2022**, *34*, 37–46. [CrossRef]

22. Gao, H.; Li, Z.; Liu, F.; Wu, Y.; Li, P.; Zhao, X.; Li, F.; Guo, J.; Liu, C.; Pan, B.; et al. Terrace formation and river valley development along the lower Taohe River in central China. *Geomorphology* **2020**, *348*, 106885. [CrossRef]

23. Pan, B.; Su, H.; Hu, Z.; Hu, X.; Gao, H.; Li, J.; Kirby, E. Evaluating the role of climate and tectonics during non-steady incision of the Yellow River: Evidence from a 1.24Ma terrace record near Lanzhou, China. *Quat. Sci. Rev.* **2009**, *28*, 3281–3290. [CrossRef]

24. Chen, J.; Dai, F.; Yao, X. Holocene debris-flow deposits and their implications on the climate in the upper Jinsha River valley, China. *Geomorphology* **2008**, *93*, 493–500. [CrossRef]

25. Tang, C.; Rengers, N.; van Asch, T.W.J.; Yang, Y.H.; Wang, G.F. Triggering conditions and depositional characteristics of a disastrous debris flow event in Zhouqu city, Gansu Province, northwestern China. *Nat. Hazards Earth Syst. Sci.* **2011**, *11*, 2903–2912. [CrossRef]

26. Tang, C.; van Asch, T.W.J.; Chang, M.; Chen, G.Q.; Zhao, X.H.; Huang, X.C. Catastrophic debris flows on 13 August 2010 in the Qingping area, southwestern China: The combined effects of a strong earthquake and subsequent rainstorms. *Geomorphology* **2012**, *139–140*, 559–576. [CrossRef]

27. Chen, X.; Cui, Y. The formation of the Wulipo landslide and the resulting debris flow in Dujiangyan City, China. *J. Mt. Sci.* **2017**, *14*, 1100–1112. [CrossRef]

28. Aucelli, P.P.C.; Casciello, E.; Cesarano, M.; Perriello Zampelli, S.; Rosskopf, C.M. A deep, stratigraphically and structurally controlled landslide: The case of Mount La Civita (Molise, Italy). *Landslides* **2013**, *10*, 645–656. [CrossRef]

29. Thanh, L.N.; De Smedt, F. Slope stability analysis using a physically based model: A case study from A Luoi district in Thua Thien-Hue Province, Vietnam. *Landslides* **2014**, *11*, 897–907. [CrossRef]